

# First-principles thermodynamic framework for the evaluation of thermochemical H<sub>2</sub>O- or CO<sub>2</sub>-splitting materials

B. Meredig and C. Wolverton\*

*Department of Materials Science and Engineering, Northwestern University, Evanston, Illinois 60208, USA*  
(Received 28 August 2009; revised manuscript received 23 November 2009; published 28 December 2009)

We present an analysis of the equilibrium thermodynamics of two-step metal oxide-based water and carbon dioxide-splitting cycles. Within this theoretical framework, we propose a first-principles computational approach based on density-functional theory (DFT) for evaluating new materials for these cycles. Our treatment of redox-based gas-splitting chemistry is completely general so that the thermodynamic conclusions herein hold for all materials used for such a process and could easily be generalized to any gas as well. We determine the temperature and pressure regimes in which the thermal reduction (TR) and gas-splitting (GS) steps of these cycles are thermodynamically favorable in terms of the enthalpy and entropy of oxide reduction, which represents a useful materials design goal. We show that several driving forces, including low TR pressure and a large positive solid-state entropy of reduction of the oxide, have the potential to enable future, more promising two-step gas-splitting cycles. Finally, we demonstrate a practical computational methodology for efficiently screening new materials for gas-splitting applications and find that first-principles DFT calculations can provide very accurate predictions of high-temperature thermodynamic properties relevant to gas splitting.

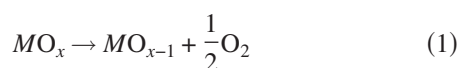
DOI: 10.1103/PhysRevB.80.245119

PACS number(s): 82.60.-s, 64.70.qd, 71.15.Mb, 63.20.-e

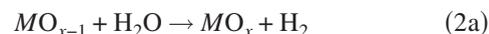
## I. INTRODUCTION

Water thermolysis is a promising means to produce hydrogen by thermochemically splitting water molecules. Carbon dioxide splitting generates CO, a hydrocarbon fuel precursor,<sup>1,2</sup> and the decomposition of CO<sub>2</sub> is also interesting for reducing greenhouse gas emissions.<sup>3,4</sup> However, *directly* decomposing H<sub>2</sub>O with thermal energy requires impractical temperatures of about 4300 K,<sup>5</sup> as well as a gas separation mechanism,<sup>6,7</sup> and a similarly discouraging picture also exists for CO<sub>2</sub>.<sup>2</sup> The most popular approach for increasing yield in the CO<sub>2</sub>-splitting community has been the use of membrane reactors<sup>1-4</sup> that continually remove CO product to keep the system out of equilibrium. Recent work in the water-splitting field, on the other hand, has generally focused on identifying materials that can reversibly participate in a lower-temperature redox cycle whose net output is H<sub>2</sub> +  $\frac{1}{2}$ O<sub>2</sub>; an analogous process can be envisioned for splitting CO<sub>2</sub>. Such a redox cycle can, in principle, have an arbitrary number of steps; the larger the number of steps, the lower the temperatures needed for each but the lower the cycle's maximum thermodynamic efficiency.<sup>8</sup> Thus, two-step (or, in some instances, three-step<sup>9</sup>) cycles seem to represent the best combination of feasible reaction temperatures and thermodynamic efficiency.

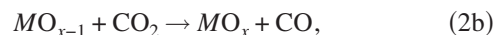
In a typical two-step gas-splitting (GS) cycle, the subject of this work, an oxide material is reduced at very high temperature (up to 2000 K). Then, the material reoxidizes by reacting with H<sub>2</sub>O or CO<sub>2</sub> and generating H<sub>2</sub> or CO (at around 1000 K). These materials often are metal oxides and the two reaction steps can be represented as



and



or



where  $M$  is a metal,  $MO_x$  is the corresponding metal oxide, and  $MO_{x-1}$  is the reduced oxide. Reaction 1 is called the thermal reduction (TR) step and reaction 2 is the GS step.

Although reactions 1 and 2 are written schematically in terms of simple binary, stoichiometric line compounds, they can represent much more complex situations as well, e.g., off-stoichiometric phases, solution phases, and multicomponent oxide materials. For instance,  $M$  might generally represent a combination of metals, and  $MO_{x-1}$  the reduced oxide products, which could be a mixture of an arbitrary number of compounds or solution phases. In a simple case,  $MO_x$  might represent 2CeO<sub>2</sub> and  $MO_{x-1}$  would represent Ce<sub>2</sub>O<sub>3</sub>. In a more complex case, where  $MO_x$  is 3CoFe<sub>2</sub>O<sub>4</sub> and a two-step decomposition takes place,<sup>10</sup>  $MO_{x-1}$  would be (2Fe<sub>3</sub>O<sub>4</sub> + 3CoO) for the first stage; these products are then reduced again in the second stage. We return to the issue of off-stoichiometric and solution phases below.

The purpose of this paper is to elucidate the factors entering the thermodynamics of a general two-step gas-splitting cycle and then to present a computational approach for predicting the thermodynamics of gas-splitting materials. First-principles calculations have never before been applied to the evaluation of gas-splitting materials. There are many previous discussions in the literature of the thermodynamics of *particular* water-splitting cycles, for example, in the form of new cycle proposals,<sup>6,11-13</sup> material-specific analyses,<sup>14-18</sup> and reviews.<sup>5,8,19-23</sup> Of particular note is Abanades *et al.*'s (Ref. 9) analysis of 280 proposed water-splitting methods, some of which are quite exotic, based on thermodynamics as well as other factors.<sup>9</sup> Discussions of carbon dioxide splitting are much less numerous but such a process is exactly analogous to water splitting; reducing CO<sub>2</sub> has a lower energetic

cost above 800 °C and reducing H<sub>2</sub>O becomes more facile below 800 °C.<sup>10</sup>

While the above studies all focus on the thermodynamic functions of specific metal redox couples, we instead construct a *general* framework for driving forces which contribute to thermodynamically spontaneous two-step gas-splitting cycles. Our framework establishes quantitative regimes for operating temperatures and pressures, as well as the enthalpy and entropy differences between MO<sub>x</sub> and MO<sub>x-1</sub> that provide favorable thermodynamics for H<sub>2</sub>O and CO<sub>2</sub> splitting. Using thermodynamic databases, we apply the results of our analysis to 105 binary oxide redox reactions. We find that all of these cycles possess either thermodynamically unfavorable TR or GS reactions (or both). However, several of these binary oxides are presently used with some success in water-splitting processes, indicating that nonequilibrium and kinetics considerations are especially important in enabling the reactions to occur. We emphasize that the present work focuses on materials thermodynamics, which we view as an important initial screening criterion for gas-splitting materials; kinetics would represent a subsequent and also very important criterion. In any case, finding new materials with more favorable thermodynamics would certainly be beneficial, so we use our framework to provide some guidance for future materials selection. Additionally, we apply density-functional theory (DFT) calculations to predict the high-temperature thermodynamic properties of several gas-splitting materials and show that they agree very well with experiment. We therefore suggest that first-principles methods may be used for screening candidate gas-splitting materials.

## II. TEMPERATURE RANGES FAVORABLE FOR BOTH TR AND GS

Ideally, one would like both the TR and GS reactions to be thermodynamically favorable, with negative Gibbs free energies of reaction. Because the steps run at different temperatures that criterion can be met in certain  $T_{\text{TR}}$  and  $T_{\text{GS}}$  ranges, where  $T_{\text{TR}}$  is the TR step temperature and  $T_{\text{GS}}$  is the GS temperature. This observation has been made in previous material-specific analyses (e.g., Kodama and Gokon's review<sup>19</sup>) but here, we examine the thermodynamics for a general two-step cycle. To find the temperatures associated with favorable energetics, the equilibrium thermodynamic expressions

$$\Delta G_{\text{TR},T_{\text{TR}}} = \Delta H_{\text{TR},T_{\text{TR}}} - T \cdot \Delta S_{\text{TR},T_{\text{TR}}} \leq 0 \quad (3)$$

and

$$\Delta G_{\text{GS},T_{\text{GS}}} = \Delta H_{\text{GS},T_{\text{GS}}} - T \Delta S_{\text{GS},T_{\text{GS}}} \leq 0 \quad (4)$$

must be satisfied. The notation we adopt here and maintain throughout is that a TR or GS subscript indicates which of the two steps is under consideration while a  $T_{\text{TR}}$  or  $T_{\text{GS}}$  subscript specifies the temperature at which each thermodynamic quantity is computed. The enthalpies and entropies in Eqs. (3) and (4) can be expressed in terms of those of the chemical reactants and products (heats of formation  $\Delta H_f$ , or

the enthalpies of the compounds relative to the composition-weighted average of the constituent elements, and standard entropies  $S$ ) in reactions 1 and 2

$$\begin{aligned} \Delta G_{\text{TR},T_{\text{TR}}} &= \Delta H_{f,T_{\text{TR}}}^{MO_{x-1}} - \Delta H_{f,T_{\text{TR}}}^{MO_x} - T_{\text{TR}} \\ &\times \left( S_{T_{\text{TR}}}^{MO_{x-1}} + \frac{1}{2} S_{T_{\text{TR}}}^{O_2} - S_{T_{\text{TR}}}^{MO_x} \right) \leq 0 \end{aligned} \quad (5)$$

and

$$\begin{aligned} \Delta G_{\text{GS},T_{\text{GS}}} &= \Delta H_{f,T_{\text{GS}}}^{MO_x} - \Delta H_{f,T_{\text{GS}}}^{MO_{x-1}} - \Delta H_{f,T_{\text{GS}}}^{H_2O} \\ &- T_{\text{GS}} (S_{T_{\text{GS}}}^{MO_x} + S_{T_{\text{GS}}}^{H_2} - S_{T_{\text{GS}}}^{MO_{x-1}} - S_{T_{\text{GS}}}^{H_2O}) \leq 0 \end{aligned} \quad (6a)$$

or

$$\begin{aligned} \Delta G_{\text{GS},T_{\text{GS}}} &= \Delta H_{f,T_{\text{GS}}}^{MO_x} - \Delta H_{f,T_{\text{GS}}}^{MO_{x-1}} - \Delta H_{f,T_{\text{GS}}}^{CO_2} \\ &- T_{\text{GS}} (S_{T_{\text{GS}}}^{MO_x} + S_{T_{\text{GS}}}^{CO} - S_{T_{\text{GS}}}^{MO_{x-1}} - S_{T_{\text{GS}}}^{CO_2}) \leq 0. \end{aligned} \quad (6b)$$

In these relations,  $T_{\text{TR}}$  and  $T_{\text{GS}}$  are chosen reaction temperatures and any properties relating to MO<sub>x</sub> and MO<sub>x-1</sub> are variables that depend on the materials used. The other material-independent quantities are well characterized experimentally. We next analyze the above expressions, first neglecting the solid-state entropies that appear and subsequently, including them.

### A. Neglecting solid-state entropy

Both the enthalpies and entropies of the oxide species appear in Eqs. (5) and (6) but to simplify the analysis, it would be convenient to eliminate the solids' entropies. Thus, the approximation

$$S^{MO_{x-1}} - S^{MO_x} \approx 0 \quad (7)$$

will be used for now (and later relaxed). That is, we assume here that the difference in solid-state entropies between the oxide and its reduced form is small, especially as compared to the gaseous species in the TR and GS reactions. The notational substitution

$$\Delta H_f^{MO_{x-1}} - \Delta H_f^{MO_x} \equiv \Delta H_{\text{reduction}} \quad (8)$$

will also prove useful since this quantity (assumed temperature independent) appears in both Eqs. (5) and (6). Applying Eqs. (7) and (8) leaves

$$\Delta G_{\text{TR},T_{\text{TR}}} = \Delta H_{\text{reduction}} - T_{\text{TR}} \frac{1}{2} S_{T_{\text{TR}}}^{O_2} \leq 0 \quad (9)$$

and

$$\Delta G_{\text{GS},T_{\text{GS}}} = -\Delta H_{\text{reduction}} - \Delta H_{f,T_{\text{GS}}}^{H_2O} - T_{\text{GS}} (S_{T_{\text{GS}}}^{H_2} - S_{T_{\text{GS}}}^{H_2O}) \leq 0 \quad (10a)$$

or

$$\Delta G_{\text{GS},T_{\text{GS}}} = -\Delta H_{\text{reduction}} - \Delta H_{f,T_{\text{GS}}}^{CO_2} - T_{\text{GS}} (S_{T_{\text{GS}}}^{CO} - S_{T_{\text{GS}}}^{CO_2}) \leq 0. \quad (10b)$$

Of interest are the TR and GS temperature ranges in which both steps have negative Gibbs free energies of reaction. Setting Eqs. (9) and (10) equal to zero will give the boundary between the thermodynamically favorable and unfavorable regions. Adding the two equations cancels out the only material-dependent property ( $\Delta H_{reduction}$ ); then, defining  $\Delta T = T_{TR} - T_{GS}$ , defining  $\Delta S$  as the increase in entropy of  $O_2$  upon heating from  $T_{GS}$  to  $T_{TR}$ , and using the definition of the Gibbs free energy of formation of  $H_2O$ , we have

$$\begin{aligned} \Delta T &= \frac{-2\Delta G_{f,T_{GS}}^{H_2O} - T_{GS}\Delta S}{S_{T_{TR}}^{O_2}} \\ &\approx \frac{-2\Delta G_{f,T_{GS}}^{H_2O}}{S_{T_{TR}}^{O_2}} \\ &\Rightarrow S_{T_{TR}}^{O_2} \Delta T \\ &\approx -2\Delta G_{f,T_{GS}}^{H_2O} \end{aligned} \quad (11a)$$

or

$$\begin{aligned} \Delta T &= \frac{-2\Delta G_{f,T_{GS}}^{CO_2} - T_{GS}\Delta S}{S_{T_{TR}}^{O_2}} \\ &\approx \frac{-2\Delta G_{f,T_{GS}}^{CO_2}}{S_{T_{TR}}^{O_2}} \\ &\Rightarrow S_{T_{TR}}^{O_2} \Delta T \\ &\approx -2\Delta G_{f,T_{GS}}^{CO_2}. \end{aligned} \quad (11b)$$

Based on experimental thermodynamic data,<sup>24</sup> the  $\Delta S$  term represents a 6% fraction of the numerator for TR at 2000 K and GS at 1000 K for  $H_2O$  splitting, or 13% for  $CO_2$ , and can be neglected in a rough approximation. Equation (11) gives the value of  $\Delta T$  for which there is exactly zero thermodynamic driving force for both reactions; wider TR-GS temperature differences are required to have thermodynamically favored reactions. We note the following regarding Eq. (11): first, there are no material-dependent properties in the expression. Thus, the size of the temperature difference between TR and GS reactions is independent of material choice, neglecting solid-state entropy. The lack of material-dependent properties also makes extension of Eq. (11) to reduction of other gases besides  $H_2O$  and  $CO_2$  quite trivial. Second, the criteria for favorable TR and GS are apparent:  $\Delta T$  and the entropy of  $O_2$  serve as driving forces whose product must equal or exceed twice the free energy of formation of  $H_2O$  or  $CO_2$ , which is the barrier to a thermodynamically preferred two-step cycle. Given that the entropy of  $O_2$  increases with temperature, we would expect the  $\Delta T$  temperature window should decrease in size for increasing TR temperature (or, conversely,  $\Delta T$  should widen as the TR temperature is lowered). Also, the favorable thermodynamics window  $\Delta T$  shrinks to zero at the temperature  $T = T_{TR} = T_{GS}$ , where  $\Delta G_f^{H_2O} = 0$  or  $\Delta G_f^{CO_2} = 0$ , corresponding to the direct, one-step thermal splitting of the gases. These conclusions agree with Miller *et al.*'s observations<sup>10</sup> for water splitting

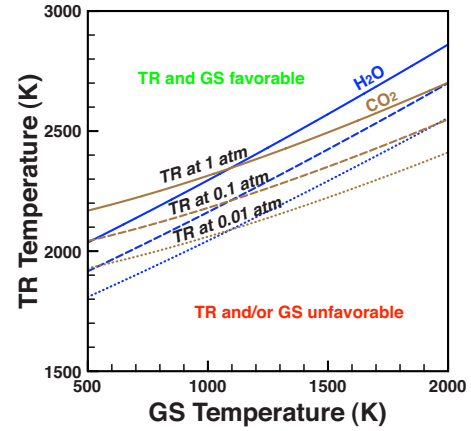


FIG. 1. (Color online) Temperature and pressure ranges in which TR and GS are thermodynamically favorable, neglecting solid-state entropy [from Eq. (11)]. The window in which both TR and GS are favorable is restrictive from experimental and materials standpoints.

that a large positive TR entropy (mostly provided by  $O_2$ ) is desirable and that running TR and GS at the same temperature implies  $\Delta G_{TR}$  and  $\Delta G_{GS}$  must have opposite signs and sum to  $\Delta G_f^{H_2O}$ .

We plot the relationship between thermodynamically allowed  $T_{TR}$  and  $T_{GS}$  [Eq. (11)] for  $H_2O$  and  $CO_2$  in Fig. 1. We find the optimal window for thermodynamics is quite restrictive, especially in light of realistic experimental TR and GS temperatures. This result agrees with previous efforts for water splitting that found no two-step oxide cycles to be practical below 1373 K (Ref. 25) and the use of three steps to be necessary for any cycle operating below 1000 K.<sup>26</sup> We reiterate that this conclusion is independent of the choice of material and is a simple function of the thermodynamics of  $H_2O$ ,  $CO_2$ , and their constituents. Figure 1 also indicates the beneficial effects of lowering the TR pressure, which we discuss in more detail below.

In addition to thermodynamic considerations, there are also practical restrictions on the useful temperature ranges which may be considered in a real two-step gas-splitting reactor. Materials may be highly volatile or suffer irreversible degradation at very high TR temperatures ( $>2000$  K) and kinetic processes will be very slow at very low GS temperatures ( $<1000$  K). These practical issues argue for reduced values of  $\Delta T$ ; however, the simple thermodynamic analysis leading to Fig. 1 shows that small values of  $\Delta T$  are only achievable thermodynamically for very high values of  $T_{TR}$  if solid-state entropy is not considered. We later show that solid-state entropy represents an additional penalty for most materials but we argue that it should be possible to tailor a material that benefits from a positive entropy change upon reduction.

## B. Pressure effects

Equation (11) is plotted in Fig. 1 for TR pressures of 1, 0.1, and 0.01 atm. Pressure effects can be incorporated by treating oxygen as an ideal gas and simply including a  $-\ln(P)$  term in Eq. (9). Pressure is not expected to play a

major role in adjusting the thermodynamics of GS, as gases appear on both sides of the reaction. During TR, however, a partial vacuum can be used to help drive oxygen release<sup>27</sup> and Fig. 1 indicates the magnitude of these pressure effects on the ideal thermodynamic operating window.

### C. Effect of solid-state entropy

Up to this point, the present analysis has neglected the role of the solid-state entropy difference between the two oxide materials. Returning to Eqs. (5) and (6), and relaxing the entropy assumption, we now introduce another materials property (assumed temperature independent),

$$S^{MO_{x-1}} - S^{MO_x} \equiv \Delta S_{reduction}. \quad (12)$$

Equations (5) and (6) then become

$$\Delta G_{TR, T_{TR}} = \Delta H_{reduction} - T_{TR} \left( \Delta S_{reduction} + \frac{1}{2} S_{T_{TR}}^{O_2} \right) \leq 0 \quad (13)$$

and

$$\begin{aligned} \Delta G_{GS, T_{GS}} = & -\Delta H_{reduction} - \Delta H_{f, T_{GS}}^{H_2O} \\ & - T_{GS} (-\Delta S_{reduction} + S_{T_{GS}}^{H_2} - S_{T_{GS}}^{H_2O}) \leq 0 \end{aligned} \quad (14a)$$

or

$$\begin{aligned} \Delta G_{GS, T_{GS}} = & -\Delta H_{reduction} - \Delta H_{f, T_{GS}}^{CO_2} \\ & - T_{GS} (-\Delta S_{reduction} + S_{T_{GS}}^{CO} - S_{T_{GS}}^{CO_2}) \leq 0. \end{aligned} \quad (14b)$$

Similarly, the  $\Delta T$  expression from Eq. (11) can be modified to include  $\Delta S_{reduction}$ ,

$$\Delta T = \frac{-2\Delta G_{f, T_{GS}}^{H_2O} - T_{GS}\Delta S}{S_{T_{TR}}^{O_2} + 2\Delta S_{reduction}} \quad (15a)$$

or

$$\Delta T = \frac{-2\Delta G_{f, T_{GS}}^{CO_2} - T_{GS}\Delta S}{S_{T_{TR}}^{O_2} + 2\Delta S_{reduction}}. \quad (15b)$$

Equation (15) indicates that a positive  $\Delta S_{reduction}$  reduces the  $\Delta T$  needed for favorable TR and GS. However, if  $\Delta S_{reduction}$  is negative (as it is in most elemental oxides), it tends to counteract the thermodynamic driving force of  $O_2$  entropy. The thermodynamically favorable TR-GS temperature window is plotted in Fig. 2 for several constant values of  $\Delta S_{reduction}$ . The plot demonstrates that large positive values of  $\Delta S_{reduction}$  can greatly improve the energetics of a two-step gas-splitting cycle. Thus,  $\Delta S_{reduction}$  must be considered an important materials design variable along with, as we later show,  $\Delta H_{reduction}$ .

### III. OPTIMIZING THE ENERGETICS OF TR AND GS

The ultimate goals of this analysis are to provide quantitative targets for the ideal thermodynamic properties of oxide

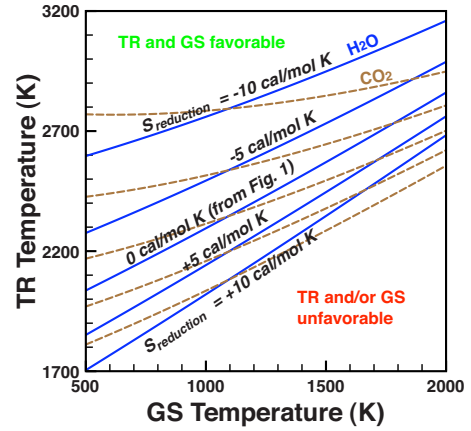


FIG. 2. (Color online) Temperature ranges in which TR (at 1 atm pressure) and GS are thermodynamically favorable, for a set of reasonable  $\Delta S_{reduction} = S^{MO_{x-1}} - S^{MO_x}$  values. This solid-state entropy delta can, if it is large and positive, broaden the window in which TR and GS are both favorable.

materials used in two-step gas-splitting cycles and then to show that computational methods may be used to predict the thermodynamics of proposed gas-splitting cycles. Presently employed gas-splitting materials do, of course, function even if one or both steps have unfavorable equilibrium thermodynamics—some product will always be observed regardless of the values of  $\Delta G_{TR}$  and  $\Delta G_{GS}$ , and nonequilibrium techniques can push reactions in the desired direction—but lowering  $\Delta G_{TR}$  and  $\Delta G_{GS}$  would certainly enhance the cycles' performance. Allendorf *et al.*,<sup>18</sup> for example, discuss both equilibrium considerations and the great importance of nonequilibrium factors in practical solar thermochemical water-splitting processes. Here we are concerned with defining the  $\Delta H_{reduction}$  and  $\Delta S_{reduction}$  regimes that make both TR and GS thermodynamically favorable, and then determining whether any binary oxides fall in that window. This ideal window, found by simultaneously satisfying Eqs. (13) and (14), is shown in Fig. 3, along with experimental data<sup>24</sup> for 105 binary oxides.

Among the oxides shown in Fig. 3 are the  $Fe_3O_4$ ,<sup>7,9,14,16,21</sup>  $CeO_2$ ,<sup>29</sup>  $Mn_3O_4$ ,<sup>14,16</sup>  $Co_3O_4$ ,<sup>14</sup>  $Nb_2O_5$ ,<sup>14</sup>  $WO_3$ ,<sup>19</sup>  $SnO_2$ ,<sup>9</sup>  $In_2O_3$ ,<sup>9</sup>  $CdO$ ,<sup>16</sup> and  $ZnO$ .<sup>9,11,21</sup> cycles that have generated interest in the water thermolysis community. Interestingly, these materials are identified as some of the best in our framework. They tend to cluster near the TR and GS equilibrium lines, where neither reaction is excessively penalized in favor of the other. Most also favor GS slightly, which is sensible given that the lower-temperature GS reaction is more likely to suffer from slow kinetics. We conclude that, in general, if one step of the cycle must be thermodynamically unfavorable, the TR reaction should be selected since it will more likely have fast kinetics and can be enhanced by low-pressure conditions.

At this point it is important to recognize that until we add specific redox data points to Fig. 3, all steps in our analysis have been entirely general. The material-specific thermodynamic data to which we have access allow us to model TR and GS reactions between stoichiometric line compounds; however, it is a simple matter to include data on this plot for

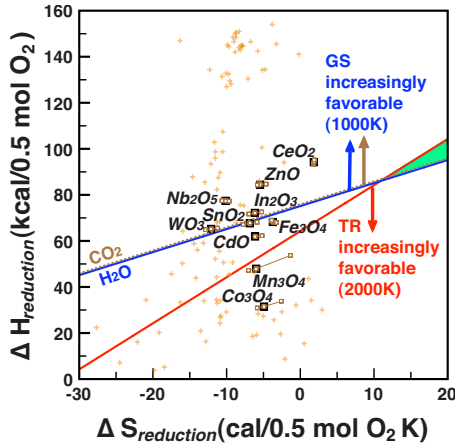


FIG. 3. (Color online) Regions of favorable TR (below indicated TR line) and GS (above indicated GS lines) thermodynamics plotted in terms of materials properties  $\Delta S_{reduction}$  and  $\Delta H_{reduction}$ , assuming TR at 2000 K and GS at 1000 K. The thermodynamics of 105 elemental oxide cycles are calculated at an intermediate temperature of 1500 K (or the next-highest available temperature in 100 K increments) from the SSUB3 database at 1 bar (Ref. 24) or in the case of Fe and its oxides from NIST (Ref. 28). Labeled cycles have generated significant interest in the literature. Brackets on those materials' points indicate the small effects of changing the assumed 1500 K temperature by  $\pm 200$  K (exceptions due to limited data:  $Fe_2O_4$  range 1300–1600 K,  $CdO$  range 1200–1400 K, and  $ZnO$  range 1300–1600 K). All the indicated materials except  $CeO_2$  move left at higher temperatures.

nonstoichiometric systems or solution phases. This possibility is discussed more in a later section. We show in Fig. 3 that none of the considered reactions achieve the proper combination of  $\Delta H_{reduction}$  and  $\Delta S_{reduction}$  needed to enable favorable TR and GS energetics. However, we note that  $\Delta S_{reduction}$  serves to open the ideal window for values greater than 10 cal/0.5 mol  $O_2$  K. Achieving a large positive  $\Delta S_{reduction}$  will be nontrivial since  $MO_{x-1}$  has fewer atoms than  $MO_x$  (and hence, fewer vibrational degrees of freedom) but Fig. 3 shows that even a few binary oxides already have  $\Delta S_{reduction} \geq 0$ . Phase transformations have the potential to contribute to  $\Delta S_{reduction}$ , although even melting of  $MO_{x-1}$  (which occurs in many of the points plotted in Fig. 3) does not supply the necessary  $\Delta S_{reduction} \geq 10$  cal/0.5 mol  $O_2$  K. Furthermore, phase transitions may lead to great engineering challenges for reactor design. Thus, an open challenge for the oxide-based gas-splitting community is to identify or develop materials that possess a large positive  $\Delta S_{reduction}$  and also a corresponding  $\Delta H_{reduction}$  based on Eqs. (13) and (14). Finally, brackets on select points in Fig. 3 are used to demonstrate the generally very slight temperature dependences of  $\Delta H_{reduction}$  and  $\Delta S_{reduction}$ , corroborating our earlier temperature-independent assumption for these properties.

#### IV. FIRST-PRINCIPLES PREDICTION OF GAS-SPLITTING THERMODYNAMICS

Since, as we have discussed above, much room exists for improving the materials thermodynamics of gas-splitting

cycles, a method for efficiently screening proposed gas-splitting materials is desirable. We next apply DFT calculations to the problem of predicting the  $\Delta H_{reduction}$  and  $\Delta S_{reduction}$  for gas-splitting materials, such that new materials can be added to the thermodynamic map of Fig. 3.

#### A. Computational methods

All DFT (Refs. 30 and 31) calculations were performed with the Vienna *ab initio* simulation package (VASP).<sup>32,33</sup> We used the Perdew-Wang 1991 (PW91) parametrization<sup>34</sup> of the generalized gradient approximation (GGA) to the DFT exchange-correlation functional. The atomic potentials we employed were constructed with Blöchl's projector augmented wave method;<sup>35,36</sup> the Mg potential treats semicore  $p$  electrons as part of the valence. All calculations involved a 550 eV energy cutoff for the plane-wave basis set and a gamma-centered  $k$ -point mesh at a density of 4000 points per reciprocal atom for semiconductors and insulators or 10 000 points per reciprocal atom for metals. Occupancies for electronic states were generally determined using Methfessel-Paxton smearing<sup>37</sup> with a width of 0.2 eV. Forces were converged to within a very stringent 5 meV/Å and to further improve the accuracy of the forces, an additional, denser support grid was introduced for augmentation charges. Finally, the interpolation scheme of Vosko *et al.*<sup>38</sup> was employed for the PW91 correlation functional.

Reaction enthalpies were determined from DFT total-energy calculations. Each material's 0 K enthalpy was corrected for zero-point energy and adjusted with temperature based on its predicted heat capacity, using the results of our phonon calculations. Because GGA is known to significantly overestimate the binding energy of  $O_2$ , a correction of +1.36 eV as calculated in the VASP-PW91 work of Wang *et al.*<sup>39</sup> was applied to our  $O_2$  enthalpy. The enthalpy of  $O_2$  was made a function of temperature using experimental data<sup>24</sup> that was extrapolated down to 0 K. Vibrational entropies were determined using the Alloy Theoretic Automated Toolkit<sup>40</sup> by integrating each material's phonon density of states. Other contributions to the total entropy were neglected, which we find to be a robust assumption. We used the frozen phonon method<sup>41,42</sup> and the quasiharmonic approximation<sup>43</sup> to populate the dynamical matrix, which was then diagonalized to yield phonon modes. Within the quasiharmonic approximation, two unit-cell volumes were considered besides the equilibrium volume, with a maximum strain of 0.04 in each direction. Atomic displacements of 0.1 Å were considered. Periodic neighbors of each displaced atom were kept at least 7.5 Å apart or, in the case of  $SiO_2$ , 10 Å apart; these criteria determined the supercell size for each material. Energy and force convergence for each material were ensured by examining a representative supercell that included an atomic displacement (as opposed to the bulk material); a higher energy cutoff of 650 eV and a threefold-denser  $k$ -point mesh were separately tested. For each material, the absolute supercell energy did not change by more than 4 meV/atom and the magnitudes of the forces on each atom did not change by more than our convergence criterion of 5 meV/Å.

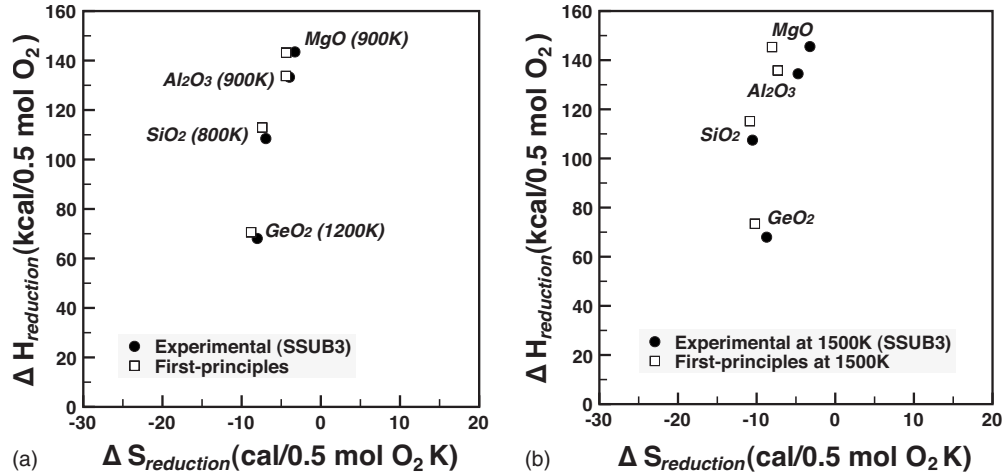


FIG. 4. Enthalpies and entropies of reduction for four selected gas-splitting cycles. Scale is identical to that of Fig. 3. (a) Experimental and first-principles calculated values for the highest possible temperature (in 100 K increments; indicated next to the data points) before either member of each pair undergoes a phase transition. (b) Experimental and first-principles values, all at 1500 K, directly comparable to Fig. 3.

### B. Computational results

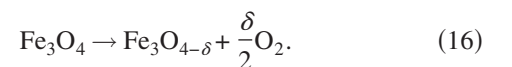
As a proof of principle, we apply DFT calculations to the gas-splitting pairs MgO-Mg,  $Al_2O_3$ -Al,  $SiO_2$ -Si, and  $GeO_2$ -Ge. We point out that these materials were selected not for their efficacy in gas splitting but rather for the sake of demonstrating the practicality of our framework. We note that transition-metal and rare-earth oxides suffer from inaccuracies within standard DFT, necessitating approaches such as DFT+ $U$  (Refs. 44 and 45) or hybrid functionals.<sup>46,47</sup> The intricacies of treating these correlated metal oxides within even the well-established DFT+ $U$  formalism remain the subject of active research.<sup>48,49</sup> As a result, we defer to a future work the application of our framework to these much more challenging materials.

The results of our calculations are shown in Fig. 4. Figure 4(a) compares experimental data<sup>24</sup> to first-principles results at the highest temperature possible before any phase transitions occur. We note that, under such conditions, the agreement between experiment and theory is excellent, even at temperatures approaching or exceeding 1000 K. Figure 4(b) contains reaction energetics at 1500 K, such that it is directly comparable to Fig. 3. Here we point out one difficulty in predicting very high-temperature thermodynamic properties from 0 K electronic structure calculations. Such calculations do not, in general, incorporate the effects of phase changes in the materials. Figure 4(b) shows the largest errors for MgO-Mg and  $Al_2O_3$ -Al; in these cycles, the metals exist experimentally as liquids at 1500 K. The experimental data thus include the heat and (more importantly) entropy of melting while the calculations do not. The smaller-magnitude thermodynamic effects of solid-state phase transitions, which appear in the experimental  $SiO_2$ -Si and  $GeO_2$ -Ge data at 1500 K are less problematic. Despite the influence of phase transitions, the calculated data in Fig. 4(b) are certainly sufficiently accurate, in light of the scale of the ideal thermodynamic window in Fig. 3, for the present computational methodology to serve as an effective screen for candidate gas-splitting materials.

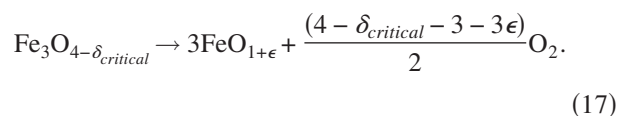
### V. EFFECTS OF OFF-STOICHIOMETRIC OXIDES, SOLUTION PHASES, AND MULTISTEP DECOMPOSITIONS

Here we comment on the full applicability of our analysis to more complex situations than the reduction and oxidation of stoichiometric line compound oxides. This discussion is motivated by the work of Allendorf *et al.*,<sup>18</sup> who considered the thermodynamics of doped ferrite spinel water splitting. Their investigation showed that allowing only the ideal, stoichiometric line compound FeO as a potential decomposition product for  $Fe_3O_4$  led to quantitatively inaccurate predictions of  $Fe_3O_4$  decomposition temperature, and emphasized the significance of including solution phases rather than only line compounds in thermodynamic modeling. We now show that the conclusions of Allendorf *et al.* are compatible with the present analysis.

Throughout this analysis, in keeping with our objective of generality, we do not exclude any potential decomposition products in favor of others. We do not assume in the form of our initial Eqs. (1) and (2) that  $Fe_3O_4$ , for example, decomposes strictly to 3FeO during TR. Without altering our framework or its conclusions, we can write  $MO_{x-\delta}$  to represent *any number of compounds or solutions* that, all together, are reduced by  $\frac{\delta}{2}$  mol  $O_2$  relative to  $MO_x$ . Our analysis thus applies to any oxygen-evolving step in the potentially complex real-world chain of reactions by which  $Fe_3O_4$  is reduced. One step could, for example, include solution phases via oxygen substoichiometry,



$\Delta H_{reduction}$  and  $\Delta S_{reduction}$  will then be functions of  $\delta$  but the framework we have developed still applies for each value of  $\delta$ . Then, once the oxygen solubility limit in  $Fe_3O_4$  is reached at some  $\delta_{critical}$ , the spinel compound decomposes into a presumably oxygen-rich FeO phase,



Clearly, our analysis may still be applied to these more complex and realistic scenarios. Indeed, the only point at which we apply the notion of a stoichiometric line compound approximation is when we add specific materials to Fig. 3 using thermodynamic data. Given such data for any solution phases of interest [e.g., the thermodynamics of Eq. (16) or Eq. (17)], those phases could be readily added to the plot as well. Furthermore, if a gas-splitting material decomposes by a multistep pathway, the above results apply to any particular oxygen-producing TR step and its corresponding gas-splitting step.

## VI. CONCLUSION

In this chemical thermodynamic analysis of oxide-based  $\text{H}_2\text{O}$  and  $\text{CO}_2$  splitting, we show that useful general conclusions can be derived for two-step cycles without limiting applicability to a particular material. We found that the quantities  $\Delta H_{\text{reduction}}$  and  $\Delta S_{\text{reduction}}$ , which represent the enthalpy and entropy differences between reduced ( $\text{MO}_{x-1}$ ) and non-reduced ( $\text{MO}_x$ ) materials participating in gas splitting, together determine the thermodynamic performance of cycles based on those materials. A material with a very large  $\Delta S_{\text{reduction}}$  could, if it also had an appropriate  $\Delta H_{\text{reduction}}$ ,

operate with favorable TR and GS thermodynamics and potentially represent a dramatic improvement over present water and carbon dioxide-splitting materials. Our identification of these ideal materials properties motivated our development of a first-principles computational approach by which we may predict the thermodynamic properties of nominally any gas-splitting cycle. We demonstrated that density-functional theory-based total-energy and frozen phonon calculations can provide reasonable descriptions of oxide thermodynamics even at the extremely high temperatures involved in gas splitting. Thus, we propose that the computational approach described here, in conjunction with the material thermodynamics targets we derived, may be used to efficiently screen gas-splitting cycles.

## ACKNOWLEDGMENTS

The authors would like to thank M. D. Allendorf, J. E. Miller, and E. B. Stechel for helpful conversations. The authors gratefully acknowledge support from a Laboratory Directed Research and Development program at Sandia National Laboratories, in the form of a Grand Challenge project entitled Reimagining Liquid Transportation Fuels: Sunshine to Petrol. Sandia is a multiprogram laboratory operated by Sandia Corporation, a Lockheed Martin company, for the United States Department of Energy, National Nuclear Security Administration under Contract No. DE-AC04-94AL85000.

\*c-wolverton@northwestern.edu

- <sup>1</sup>Y. Nigara and B. Cales, *Bull. Chem. Soc. Jpn.* **59**, 1997 (1986).
- <sup>2</sup>N. Itoh, C. Sanchez, W. Xu, K. Haraya, and M. Hongo, *J. Membr. Sci.* **77**, 245 (1993).
- <sup>3</sup>Y. Fan, J. Ren, W. Onstot, J. Pasale, T. Tsotsis, and F. Egolfopoulos, *Ind. Eng. Chem. Res.* **42**, 2618 (2003).
- <sup>4</sup>W. Jin, C. Zhang, P. Zhang, Y. Fan, and N. Xu, *AIChE J.* **52**, 2545 (2006).
- <sup>5</sup>T. Kodama, *Prog. Energy Combust. Sci.* **29**, 567 (2003).
- <sup>6</sup>A. Kogan, *Int. J. Hydrogen Energy* **23**, 89 (1998).
- <sup>7</sup>T. Nakamura, *Sol. Energy* **19**, 467 (1977).
- <sup>8</sup>C. Perkins and A. Weimer, *Int. J. Hydrogen Energy* **29**, 1587 (2004).
- <sup>9</sup>S. Abanades, P. Charvin, G. Flamant, and P. Neveu, *Energy* **31**, 2805 (2006).
- <sup>10</sup>J. Miller, M. Allendorf, R. Diver, L. Evans, N. Siegel, and J. Stuecker, *J. Mater. Sci.* **43**, 4714 (2008).
- <sup>11</sup>E. Bilgen, M. Ducarroir, M. Foex, F. Sibieude, and F. Trombe, *Int. J. Hydrogen Energy* **2**, 251 (1977).
- <sup>12</sup>H. Kaneko, N. Gokon, N. Hasegawa, and Y. Tamaura, *Energy* **30**, 2171 (2005).
- <sup>13</sup>Y. Tamaura, A. Steinfeld, P. Kuhn, and K. Ehrensberger, *Energy* **20**, 325 (1995).
- <sup>14</sup>M. Lundberg, *Int. J. Hydrogen Energy* **18**, 369 (1993).
- <sup>15</sup>R. Palumbo, J. Léde, O. Boutin, E. Elorza Ricart, A. Steinfeld, S. Möller, A. Weidenkaff, E. A. Fletcher, and J. Bielicki, *Chem. Eng. Sci.* **53**, 2503 (1998).

- <sup>16</sup>F. Sibieude, M. Ducarroir, A. Tofighi, and J. Ambriz, *Int. J. Hydrogen Energy* **7**, 79 (1982).
- <sup>17</sup>M. Sturzenegger and P. Nüesch, *Energy* **24**, 959 (1999).
- <sup>18</sup>M. Allendorf, R. Diver, N. Siegel, and J. Miller, *Energy Fuels* **22**, 4115 (2008).
- <sup>19</sup>T. Kodama and N. Gokon, *Chem. Rev.* **107**, 4048 (2007).
- <sup>20</sup>S. Licht, *Chem. Commun.* **2005**, 4635.
- <sup>21</sup>A. Steinfeld, P. Kuhn, A. Reller, R. Palumbo, J. Murray, and Y. Tamaura, *Int. J. Hydrogen Energy* **23**, 767 (1998).
- <sup>22</sup>A. Steinfeld, *Sol. Energy* **78**, 603 (2005).
- <sup>23</sup>A. W. Weimer, T. Francis, C. Carney, J. Wyss, J. Martinek, and M. Kerins, DOE Hydrogen Program FY 2006 Annual Report, 2006 (unpublished), pp. 216–219.
- <sup>24</sup>Scientific Group Thermodata Europe (SGTE) Substances Database SSUB (v.3).
- <sup>25</sup>J. E. Funk and R. M. Reinstrom, *Ind. Eng. Chem. Process Des. Dev.* **5**, 336 (1966).
- <sup>26</sup>B. M. Abraham and F. Schreiner, *Ind. Eng. Chem. Fundam.* **13**, 305 (1974).
- <sup>27</sup>R. Diver, J. Miller, M. Allendorf, N. Siegel, and R. Hogan, *ASME J. Sol. Energy Eng.* **130**, 041001 (2008).
- <sup>28</sup>M. Chase, *J. Phys. Chem. Ref. Data* **9**, 1 (1998).
- <sup>29</sup>S. Abanades and G. Flamant, *Sol. Energy* **80**, 1611 (2006).
- <sup>30</sup>P. Hohenberg and W. Kohn, *Phys. Rev.* **136**, B864 (1964).
- <sup>31</sup>W. Kohn and L. J. Sham, *Phys. Rev.* **140**, A1133 (1965).
- <sup>32</sup>G. Kresse and J. Hafner, *Phys. Rev. B* **47**, 558 (1993).
- <sup>33</sup>G. Kresse and J. Furthmüller, *Phys. Rev. B* **54**, 11169 (1996).

- <sup>34</sup>J. P. Perdew, *Electronic Structure of Solids 91* (Akademie Verlag, Berlin, 1991).
- <sup>35</sup>P. E. Blöchl, Phys. Rev. B **50**, 17953 (1994).
- <sup>36</sup>G. Kresse and D. Joubert, Phys. Rev. B **59**, 1758 (1999).
- <sup>37</sup>M. Methfessel and A. T. Paxton, Phys. Rev. B **40**, 3616 (1989).
- <sup>38</sup>S. H. Vosko, L. Wilk, and M. Nusair, Can. J. Phys. **58**, 1200 (1980).
- <sup>39</sup>L. Wang, T. Maxisch, and G. Ceder, Phys. Rev. B **73**, 195107 (2006).
- <sup>40</sup>A. van de Walle, M. Asta, and G. Ceder, Calphad **26**, 539 (2002).
- <sup>41</sup>S. Wei and M. Y. Chou, Phys. Rev. Lett. **69**, 2799 (1992).
- <sup>42</sup>G. Garbulsky, Ph.D. thesis, Massachusetts Institute of Technology, 1996.
- <sup>43</sup>G. Grimvall, in *Selected Topics in Solid State Physics*, edited by E. Wohlfarth (North-Holland, Amsterdam, 1986).
- <sup>44</sup>V. I. Anisimov, J. Zaanen, and O. K. Andersen, Phys. Rev. B **44**, 943 (1991).
- <sup>45</sup>V. I. Anisimov, F. Aryasetiawan, and A. I. Lichtenstein, J. Phys.: Condens. Matter **9**, 767 (1997).
- <sup>46</sup>J. Heyd, G. E. Scuseria, and M. Ernzerhof, J. Chem. Phys. **118**, 8207 (2003).
- <sup>47</sup>C. Adamo and V. Barone, J. Chem. Phys. **110**, 6158 (1999).
- <sup>48</sup>B. Amadon, F. Jollet, and M. Torrent, Phys. Rev. B **77**, 155104 (2008).
- <sup>49</sup>B. Dorado, B. Amadon, M. Freyss, and M. Bertolus, Phys. Rev. B **79**, 235125 (2009).